CrossMark

ORIGINAL ARTICLE

Stochastic finite-fault simulation of ground motion from the August 11, 2012, M_w 6.4 Ahar earthquake, northwestern Iran

Reza Heidari

Abstract In this study, the 11 August 2012 M_w 6.4 Ahar earthquake is investigated using the ground motion simulation based on the stochastic finite-fault model. The earthquake occurred in northwestern Iran and causing extensive damage in the city of Ahar and surrounding areas. A network consisting of 58 acceleration stations recorded the earthquake within 8–217 km of the epicenter. Strong ground motion records from six significant well-recorded stations close to the epicenter have been simulated. These stations are installed in areas which experienced significant structural damage and humanity loss during the earthquake. The simulation is carried out using the dynamic corner frequency model of rupture propagation by extended fault simulation program (EXSIM). For this purpose, the propagation features of shear-wave including Q_s value, kappa value k_0, and soil amplification coefficients at each site are required. The kappa values are obtained from the slope of smoothed amplitude of Fourier spectra of acceleration at higher frequencies. The determined kappa values for vertical and horizontal components are 0.02 and 0.05 s, respectively. Furthermore, an anelastic attenuation parameter is derived from energy decay of a seismic wave by using continuous wavelet transform (CWT) for each station. The average frequency-dependent relation estimated for the region is $Q = (122 \pm 38)f^{(1.40 \pm 0.16)}$. Moreover, the horizontal to vertical spectral ratio H/V is applied to estimate the site effects at stations. Spectral analysis of the data indicates that the best match between the observed and simulated spectra occurs for an average stress drop of 70 bars. Finally, the simulated and observed results are compared with pseudo acceleration spectra and peak ground motions. The comparison of time series spectra shows good agreement between the observed and the simulated waveforms at frequencies of engineering interest.

Keywords Stochastic · Finite-fault modeling · EXSIM · Quality factor · Kappa value · CWT

1 Introduction

On August 11, 2012, two destructive earthquakes occurred a few minutes apart at Azerbaijan region of northwestern Iran (Fig. 1a). At 12:23 UTC, the first moderate event with the magnitude of M_w 6.4 (The United States Geological Survey, USGS, http://earthquake.usgs.gov/) was recorded through 58 acceleration stations with epicentral distance between 8 and about 217 km (Fig. 1). The maximum values of horizontal peak ground accelerations (PGAs) of 470 and 441 cm/s² were recorded at Satarkhan Dam and Varzaghan stations, respectively. This event ruptured an E-W striking fault in a dominantly right-lateral strike-slip faulting. Only 11 min after the first event, the second earthquake at 12:34 UTC with the magnitude of M_w 6.3 occurred with maximum horizontal PGA of almost 532 cm/s² at Varzaghan station. The second

R. Heidari (✉)
Department of Geophysics, Science and Research Branch, Islamic Azad University, Tehran, Iran
e-mail: r.heidari@srbiau.ac.ir

Fig. 1 Seismotectonic map of Iran. **a** Focal mechanisms of introduced earthquakes in this study and distribution of the studied earthquakes in Motazedian (2006) in northern Iran (e.g., Manjil M_w 7.4, 1990; Garmkhan M_w 6.5, 1997; Kojour M_w 6.3, 2004; etc.). **b** Location of the 11 August 2012 double earthquakes and their focal mechanisms. *Large black triangles* indicate the target stations, which are simulated based on their records; *small gray triangles* in the other ISMN stations and *small gray circles* show distribution of aftershocks
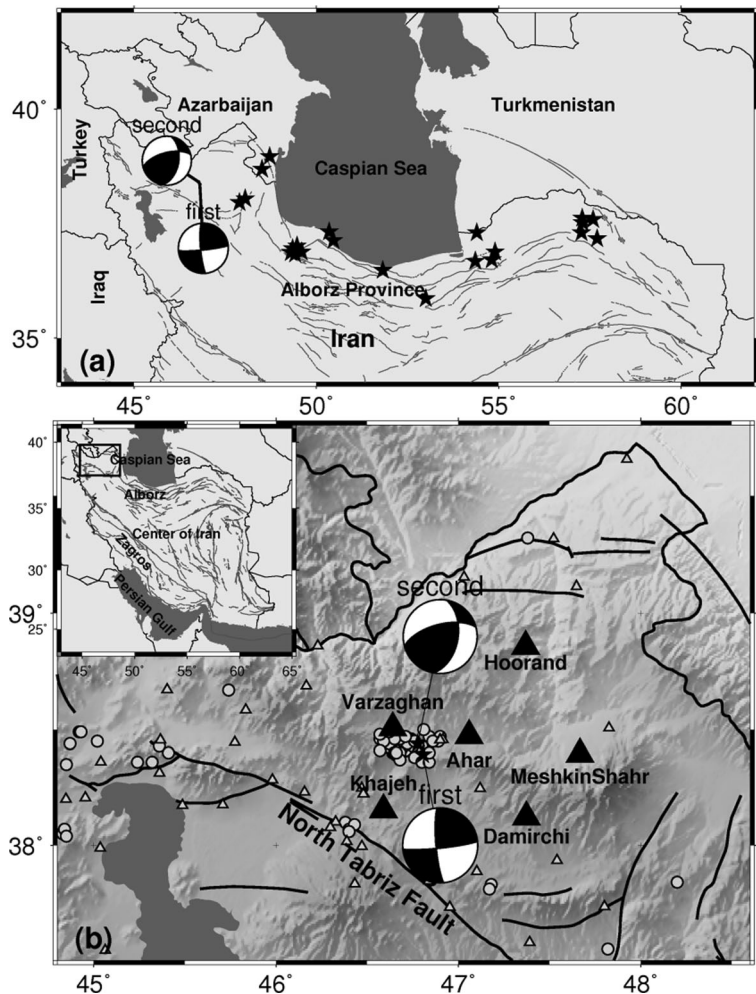
event was an oblique combination of thrust and strike-slip motion (Fig. 1). It must be noticed that Ahar-Varzaghan earthquakes occurred on an unfamiliar active fault at the north of North Tabriz Fault (NFT) (e.g., Hessami et al. 2003) in an area with no experienced significant historical and instrumental seismicity. These two events struck a wide area around Ahar and Varzaghan cities which caused the death of 300 people, about 2500 injuries, and 20 to 100 % damage to 50 villages (Bolourchi et al. 2012).

In the present study, synthetic accelerograms for the first Ahar-Varzaghan earthquake (Ahar event) are generated using the stochastic finite-fault modeling proposed by Motazedian and Atkinson (2005). In this method, the finite fault (a rectangular plane) is subdivided into a number of subfaults as point sources which radiate an ω-square model of the spectrum.

Furthermore, a simple dynamic model (Motazedian and Atkinson 2005) is used to simulate the rupture propagation, which is radially propagated at the hypocenter. For the purpose of spectral simulation of the Ahar event, the region-specific seismic parameters including anelastic attenuation, local site effects (soil amplification), and decay parameter are needed. Thus, the current study estimates these propagation characteristics. These parameters are difficult to estimate in Iran due to the presence of different seismotectonic regions (e.g., Berberian 1976; Nowroozi 1976; and Mirzaei et al. 1999). Motazedian (2006) presents the region-specific seismic parameters and stress drop at Alborz province in northern Iran by using records of 23 earthquakes whose locations are shown in Fig. 1a. The Ahar earthquake also occurred in the same region (Fig. 1). Generally, the primary purpose in this study is the

calibration of the path and source parameters of the Ahar earthquake. Moreover, the comparison of obtained region-specific seismic parameters with those predicted by the Motazedian (2006) is also interesting.

2 Tectonic setting

The current tectonics of northwestern Iran is mostly the result of the oblique exposure between the Arabia-Eurasian plates with the ratio coverage in order of 20 mm/year in Tabriz city (Vernant et al. 2004). This oblique convergence of motion leads to partitioning of the motion to shortening along Caucasus and right-lateral strike-slip movements along NFT (Jackson 1992; McClusky et al. 2000; Copley and Jackson 2006). The more recent seismicity behaviors in two Ahar-Varzaghan earthquakes highlight this partitioning (Fig. 1b; see focal mechanisms). The first event is close-ly pure right-lateral strike-slip, and another is the combination of thrust and strike-slip motions. The most significant NFT is the most striking tectonic structure in vicinity of Tabriz city with a clear WNW-ESE strike-slip motion and length of more than ~100 km. Hessami et al. (2003) and Solaymani Azad et al. (2010) suggested that this faulting system experienced at least three large earthquakes since 33.5 ka. In addition, based on historical seismicity documents, Tabriz city suffered several devastating earthquakes with magnitude of more than 6.0, imposing massive losses to human lives (Ambraseys and Melville 1982; Berberian 1994; Berberian and Yeats 1999).

Copley et al. (2013) mapped the location of the amount slip and surface faulting for the Ahar earthquake satellite images and showed that the event ruptured to the surface on a ~E-W striking fault plane with mostly right-lateral strike-slip motion. They also estimated a centroid depth of 7 km, though the rupture reached to surface and extended to about 14 km in depth. They calculated 265, 90, and 175 values for strike, dip, and rake during the Ahar earthquake, respectively. In this study, their proposed values were used as input for EXSIM.

3 Ground-motion data

The data consists of more than 190 vertical and horizontal acceleration waveforms recorded by the Iranian Strong Motion Network (ISMN) which is maintained by the Building and Housing Research Center (BHRC; http://www.bhrc.gov.ir). These accelerograms were recorded by 64 three-component accelerometers (SSA-2) with a sampling rate of 200 samples per second. The data is related to two main Ahar-Varzaghan events and an aftershock. Table 1 shows the specifications of the studied events. Among the available records in this dataset, horizontal records of the 11 August 2012 Ahar earthquake at Varzaghan, Meshkin Shahr, Damirchi, Hoorand, and Khajeh stations were selected for simulation (Fig. 1). The motioned stations are installed in areas which have experienced significant structural destruction. The relatively strong signal-to-noise ratios (SNR) of those records are significantly high, and there are good and enough records of the three motioned events to quantify the local specifications (site effects). Moreover, these stations were located within 18–75 km of the epicenter and record PGAs between 49 and 441 gal. Generally, different approaches can be applied to define rock and soil sites. The average shear-wave velocity over the top 30 m, V_{S30}, is widely used for site classification. Mousavi et al. (2014) classified 35 stations in northwestern Iran in terms of their fundamental resonance frequency. The soil information of the used six stations in this study was extracted from Mousavi et al. (2014) study. Names, locations, fault distance (R_{JB}), and V_{S30} of these stations are listed in Table 2.

In order to calculate the decay parameter k_0, both vertical and horizontal records of the two main 11 August 2012 Ahar-Varzaghan earthquakes were used (the

Table 1 List of earthquakes in this study, recorded by ISMN in NW Iran

Event no.	Month, day, year	hh:mm:ss	Latitude	Longitude	M_w	Depth (km)	Reference
First (Ahar)	August 11, 2012	12:23:15.2	38.32	46.88	6.4	9.9	USGS
Second	August 11, 2012	12:34:33.8	38.32	46.76	6.3	9.8	USGS
Aftershock	August 11, 2012	12:30:12.4	38.41	46.78	4.8[a]	6.1	IRSC

[a] M is Nuttli magnitude

Table 2 The records that were used in this study for simulation

Station name	Latitude	Longitude	R_{JB} (km)	Site class[a]	V_{S30} (m/s)
Ahar	38.474	47.059	14	**III**	275
Varzaghan	38.507	46.640	12	**III**	275
Meshkin Shahr	38.394	47.667	65	**I**	1000
Damirchi	38.123	47.373	50	–	1241
Hoorand	38.858	47.369	64	**II**	500
Khajeh	38.154	46.589	28	–	450

[a] Based on Zare et al. (1999); at these sites, generic values of 275, 500, and 1000 m/s have been assigned for V_{S30} of classes III, II, and I, respectively (shown in bold font)

aftershock records were ignored due to large scattering in the result). Furthermore, to specify soil-amplification at each station, the records of three motioned events including vertical and horizontal components were used. In order to estimate anelastic attenuation Q_s, based on features of a selected method which will be described later, only vertical components of the main Ahar event in six motioned stations were used.

After removing mean and trend, the S-wave portion of accelerograms corrected for instrument response was manually windowed. In fact, first, the S-wave arrival time is triggered using the existence velocity model of a study area and then, a window with time-duration between about 3 and 10 s relevant to hypocentral distance is selected. All of the records were tapered by using a 10 % cosine taper after windowing process and before taking the Fourier transform. The Fourier spectra were smoothed in the range of 0.1 to 20 Hz.

4 Spectral decay parameter

High-frequency amplitudes, generally more than almost 5 Hz, diminished throughout a medium (Motazedian 2006), were obtained from the slop of a smoothed Fourier spectrum of an accelerogram at linear scale of frequencies (Anderson and Hough 1984). The factor $\exp(-\pi f k)$ can be used for diminishing process of spectral amplitudes at high frequency. Atkinson (2004) believed that kappa factor is mostly a site effect. The amplitude spectra of smoothed windowed accelerogram (containing S-wave) were obtained. Then, the best line was fitted to the amplitude spectra using the least-squares method and the values of the slopes were converted to the spectral decay parameter k. Finally, kappa factor values for all records were plotted against

epicentral distances. Both vertical and horizontal components in different distances (15–200 km) were used in order to investigate the subtraction of kappa effects from a site effect in such a condition that k_v and k_h were not equal and $k_v \neq 0$ (Motazedian 2006) and also to investigate the dependency between distance and kappa factor. The best fit line $k = k_r + k_0 R$ was used to illustrate the distribution of kappa values versus distance.

These relations for vertical and horizontal components are $k = (0.0003)\,R + 0.0232\,(\pm 0.0107)$ and $k = (0.0003)\,R + 0.0489\,(\pm 0.0135)$, respectively (Fig. 2). As it is indicated in Fig. 2, the general trend of kappa factor for vertical and horizontal components is the same with different k_0, which means that the attenuation of high frequencies for the vertical components is less than that of the horizontal component. These results are in conformity with Motazedian's results (2006) indicating kappa factors for the vertical and horizontal components equal to 0.03 and 0.05 s, respectively, in the same area. The large scatter results primarily from various factors including absence of records of any large earthquakes, large station separation, and complexity of the seismic source and wave propagation characteristics in northwestern Iran. Moreover, the attenuation of high frequencies is sensitive to the variation of shear-wave velocity of near-surface deposits. As listed in Table 2, the shear-wave velocities of six sampled stations are significantly varied in different places in the study area.

5 Site effect

During propagation of earthquake waves from the source to station, the amplitude spectrum is amplified due to distinct seismic impedance effects for generic soft-rock sites (Boore and Joyner 1997). Therefore, the
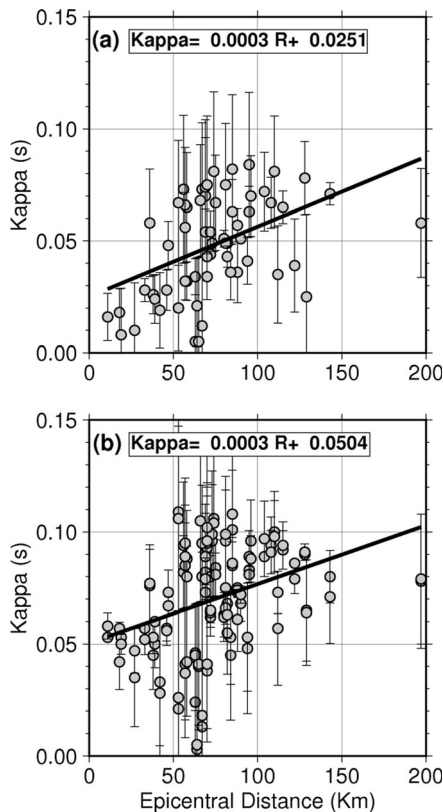
Fig. 2 The distribution of kappa factor on epicentral distance for **a** vertical components and **b** horizontal components. The k_0 value is 0.023 and 0.049 for vertical and horizontal components, respectively. Residuals are shown by *error bars*

site effect for the six stations that are used for ground motion simulation should be investigated. For this purpose, time series for three earthquakes listed in Table 1 were used. Horizontal to vertical spectral ratios (H/V) introduced by Nakamura (1989) were used to extract soil amplification at each station. Although there is no strong theory behind the H/V ratio method, good results of soil amplifications were reported by scientists (e.g., Nakamura 1989; Lermo and Chavez-Garcia 1993; Beresnev and Atkinson 1997; Atkinson and Cassidy 2000; and Siddiqqi and Atkinson 2002). The Fourier spectra of longitudinal, transverse, and vertical accelerograms for each station were estimated for at least three windows within the record (windowed S-wave) using a 30 % overlap. The amplitude spectra of the horizontal component were computed by taking the square root of the sum of squares of two longitudinal and transverse amplitude spectra. The smoothed spectra were used to obtain H/V ratio for each event. Finally, soil amplification for each station was obtained by

calculating the average of all ratios at the given frequencies. Figure 3 shows H/V ratios for six stations. Generally, the overall site effect is site amplification (H/V) multiplied by the near-surface attenuation as $H/V \exp(-\pi f k_v)$ (Motazedian 2006). The reason is that in the H/V approach, the vertical amplification is negligible, whereas the surface attenuation for vertical component is non-zero, but less than surface attenuation for the horizontal components. According to Motazedian (2006), a portion of kappa value for the horizontal component was subtracted by applying $H/V \exp(-\pi f k_v)$ to define the site effect as input for EXSIM.

6 Quality factor

Generally, quality factor represents the amplitude attenuation of propagated waves over time which occurred due to various energy-loss mechanisms relevant to
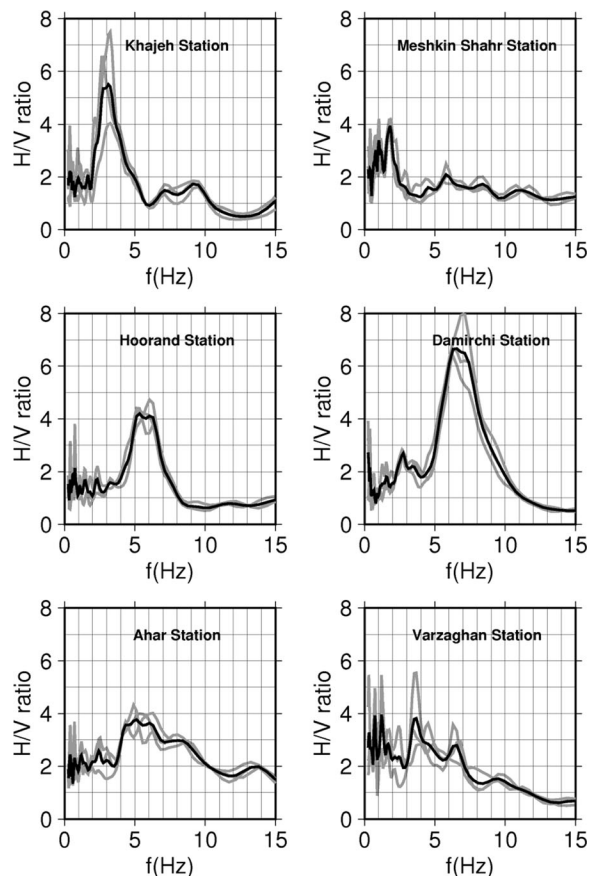

Fig. 3 The spectral H/V ratios for six target stations are shown in Fig. 1b. The *gray lines* are related to events listed in Table 1, and the *black line* illustrates their average

anelastic behaviors of the earth. This parameter was determined based on the slop of the high-frequency spectrum of earthquake records in different places which depends on the tectonic features (e.g., Aki 1980). The direct regression on the shear-wave Fourier amplitude spectra has been widely used in different regions in order to quantify the anelastic attenuation (e.g., Raoof et al. 1999; Sokolov et al. 2002; Atkinson 2004; Motazedian and Atkinson 2005; and Motazedian 2006). Motazedian (2006) obtained an attenuation factor as $Q = 87e^{1.46}$ for northern Iran where the Ahar earthquake occurred (Fig. 1). Since the vertical component is much less affected by site conditions compared to the horizontal component, Motazedian (2006) merely used the vertical components. Here, in order to obtain the anelastic attenuation parameter Q for each wave propagate path, wavelet-based analyses for accelerograms recorded during the Ahar earthquake at six target stations were applied.

The wavelet transform is a useful tool for non-stationary analysis of seismic data at various scales (Daubechies 1992). A continuous wavelet transform of a real signal $f(t)$ with respect to an analytical wavelet $\Psi(t)$ is defined as (Mallat 1999):

$$W_\Psi f(a,b) = |a|^{-1/2} \int_{-\infty}^{+\infty} f(t)\Psi\left(\frac{t-b}{a}\right)dt \qquad (1)$$

where $W_\Psi f(a,b)$ is the wavelet transform coefficient, parameters a and b are scale and translation, respectively, and the $\Psi(t)$ is an arbitrary wavelet. With such a powerful tool, one can write the anelastic amplitude diminish term for separate harmonic oscillations in time domain as:

$$A(t) = A_0 \exp\left(-\pi f t / Q\right) \qquad (2)$$

where Q is defined as fractional loss of energy per cycle of monochromic oscillation, and A and A_0 are the amplitude and its initial value of each frequency, respectively. Therefore, single-frequency energies of ground motion were extracted by applying continuous wavelet transform in order to interpret their attenuating by Eq. (2). The following steps were performed to obtain anelastic attenuation by wavelet transform: (1) the shear-wave portion of time series was windowed for all vertical components at six target stations. The Q values were calculated based on a vertical component in order to minimize the terrible effects of the site and scattering attenuation on the result. (2) After tapering by

using a 10 % cosine taper on each end of signal, the windowed time series were smoothed by using a moving average low-pass filter. (3) The decomposition yields wavelet coefficients were calculated over a total of 256 scales by using Meyer wavelet. (4) The values of the scales were converted into the frequency using Mayer wavelet features and sample rate of data (200 samples/s). Therefore, the total energy of each accelerogram is decomposed into individual frequencies which are attenuated depending on their frequencies, by quality factor (Eq. 2). (5) After taking logarithms of absolute value of the decomposed amplitudes for each frequency, the largest amplitude was chosen and its arrival time was considered as the reference time. (6) For those amplitudes that were recorded after the reference time, the best fit line to the form $\mathrm{Ln}A = \mathrm{Ln}A_0 + (-\pi f t/Q)$ was fitted to the envelope of amplitude versus time (Fig. 4a). (7) The slop values of derived lines from energy spectra at time-scale diagrams for each frequency were converted into quality factor
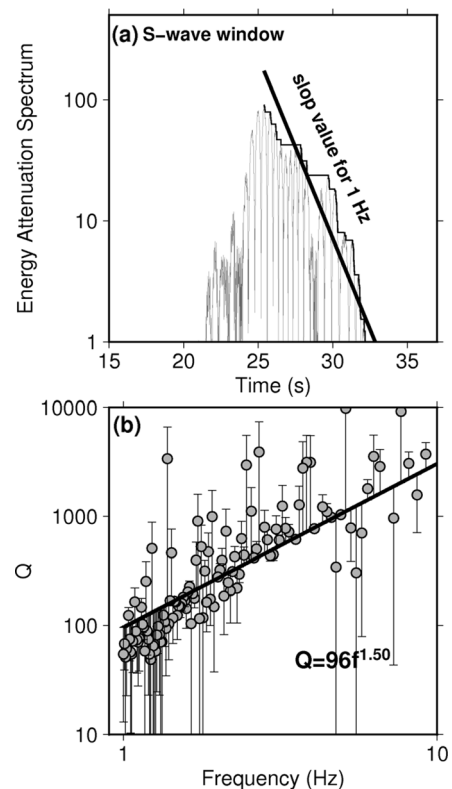

Fig. 4 For Ahar station: **a** the illustration of anelastic energy decay in time scale in wavelet scale for 1 Hz signal using Meyer wavelet, **b** the plot Q_s versus frequencies for vertical component. The best line is fitted using least-squares and indicated by the *solid line*. Residuals are shown by *error bars*

Table 3 Anelastic specifications of target stations in $Q=Q_0 f^n$ form

Station name	Relation
Ahar	$Q=96f^{1.50}$
Varzaghan	$Q=149f^{1.41}$
Meshkin Shahr	$Q=145f^{1.53}$
Damirchi	$Q=122f^{1.48}$
Hoorand	$Q=162f^{1.08}$
Khajeh	$Q=60f^{1.40}$

(slop$=-\pi f t/Q$) and plotted against the frequency content (circles in Fig. 4b) to evaluate the final form of quality factor as $Q = Q_0 f^n$. Q_0 and n parameters were determined by the least-squares method (Fig. 4b). Table 3 contains the anelastic specifications for each site which confirms Motazedian's results (2006). The average frequency dependence of Q values was estimated by $Q = (122 \pm 38) f^{(1.40\pm0.16)}$.

7 Finite-fault modeling

The stochastic finite-fault method simulates ground motion by multiplying the parametric explanations of the

ground motion's amplitude spectrum as separated various factors including source, path, and site with a random phase spectrum (Hartzell 1978; Heaton and Hartzell 1986; Joyner and Boore 1986; Beresnev and Atkinson 1998). In this approach, a large fault is divided to N number of subfaults. Next, the created ground motions of each subfault as a point-source are summed with an appropriate delay time in order to produce the ground motion of the whole rupture. The ground motion acceleration time-series, $a(t)$, is described by the following equation:

$$a(t) = \sum_{i=1}^{nl} \sum_{j=1}^{nw} a_{ij}\left(t + \Delta t_{ij}\right) \tag{3}$$

where nl and nw are the number of subfaults along the length and width of the rupture plane, respectively. $a_{ij}\left(t + \Delta t_{ij}\right)$ is the acceleration time-series for each subfault calculated by the stochastic point-source method (Boore 1983). In such method, delay time (Δt) is relevant to the time interval of propagated wave for each subfault in an observation point. According to point-source method, the ground motion of earthquake for each subfault was estimated using ω^2 model (Aki 1967) and at a hypocentral distance(D) as (Boore 1983):

Table 4 Model input parameter for the Ahar earthquake

| Input parameters	Specifications	References
Stress drop	70 bars	This study
Duration	T_0+0.1 km	Motazedian (2006)
Fault length	18 km	This study
Fault width	10 km	This study
Fault depth	7 km	This study
Strike	265°	Copley et al. (2013)
Dip	90°	Copley et al. (2013)
S-wave velocity	3.2 km/s	Motazedian (2006)
Pulsing area percentage	50 %	Motazedian (2006)
Windowing function	Saragoni-Hart	Motazedian (2006)
Rupture velocity	0.8 of β	Motazedian (2006)
Slip distribution	Random	Motazedian (2006)
H/V	$H/V\exp(-\pi f k v)$	This study
k_v	0.03	This study
Q(f)	Wavelet scales	This study
Kappa	0.05	This study
Geometric spreading	$\left\{ D < 70\text{km}\rightarrow D^{-1.0} \;\; 70 \text{ km}\leq D\leq150 \rightarrow D^{+0.2} \;\; 150 \text{ km} < D\rightarrow D^{-0.1} \right.$	Motazedian (2006)
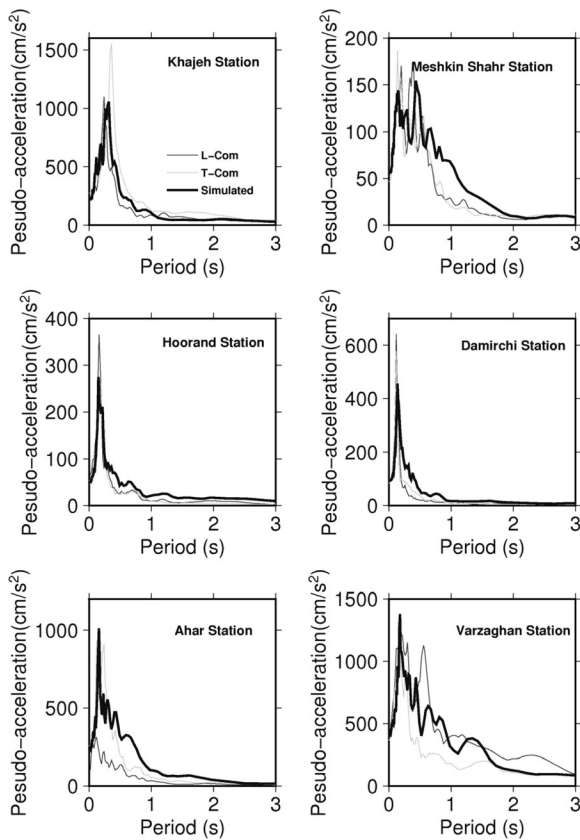
Fig. 5 The response spectra of observed and simulated acceleration time series for the 2012 Ahar earthquake in six target stations

$$A(f) = \left\{ \frac{CM_0(2\pi f)^2}{1+\frac{f^2}{f^0}} \right\} \left\{ \exp(-\pi f k) \exp\left(-\pi f D \big/ Q\beta\right) \right\} 1 \big/ D \quad (4)$$

here, M_0 is seismic moment (dyn.cm) and f_0 is corner frequency calculated by $f_0 = 4.9 \times 10^6 \beta (\Delta\sigma/M_0)^{1/3}$ for each subfault. β is the shear-wave velocity (km/s), and $\Delta\sigma$ is the stress drop (bars). The constant $C = \mathrm{R}^{\theta\varphi}FV/4\pi\rho\beta^3$ where $\mathrm{R}^{\theta\varphi}$ is the radiation pattern (average value of 0.55 for S-wave), F is the free surface amplification (2.0); V is the partitioning coefficient into two horizontal components (0.71), and ρ is the density (kg/m³) of propagating medium. The term $\exp(-\pi f k)$ represents near-surface attenuation "kappa" (Anderson and Hough 1984). Q and $1/D$ are indicated of anelastic and geometrical spreading attenuation parameters, respectively. It should be noted that the site effect term which is previously described is not considered in Eq. (4).

8 Simulation results and discussion

The acceleration time series of the Ahar earthquake that occurred on 11 August 2012 were simulated at six previously mentioned stations (Fig. 1b). In the current study, the extended earthquake fault simulation program *EXSIM* (Motazedian and Atkinson 2005) was used in order to predict ground motion. The length and width of rupture are selected based on Wells and Coppersmith (1994) as ∼18 × 10 km which conform to surface rupture of 13 km which was reported by Copley et al. (2013). According to self-similarity and scaling relations introduced by Irikura and Kamae (1994), the fault plane for the Ahar earthquake was divided into 8 × 7 segments. The best results were obtained for the rupture that propagates at $i = 1$ and $j = 5$ segments along the length and width of a fault, respectively. This indicates that the rupture started in the west and spread to the east. Motazedian (2006) showed a stress drop of 68 bars for the earthquakes in north of Iran based on both static (Beresnev and Atkinson 1998) and dynamic corner frequency (Motazedian and Atkinson 2005) approaches. This study confirms Motazedian's results (Motazedian 2006) and shows that the best result for stress drop is around 70 bars by comparing observed and simulated peak ground motions and Fourier spectra. Based on results obtained by Motazedian (2006), the source-path parameters including geometric spreading and the duration of ground motion (function of magnitude and distance) were set. Thus, the geometric spreading was considered as R^{-1} for distances less than 70 km, $R^{+0.2}$ for distances between 70 and 150 km, and $R^{-0.1}$ for larger distances. Other parameters are also listed in Table 4. Finally, ground motions were simulated. The 5 % damped response spectra were selected to compare simulated results with observations. The pseudo acceleration spectra of both observed and simulated time series are shown in Fig. 5, and their peak ground accelerations, velocities, and displacements are listed in Table 5. The frequency content of each simulated acceleration time series was compared with the actual record by the calculation of residuals. Residuals were defined as the log of observed PSA (the geometric mean of the two horizontal components) minus the log of predicted PSA. The distribution of residuals is plotted versus frequency contents in Fig. 6.

Table 5 A judgment of the observed and simulated peak ground motion of the Ahar earthquake in six target stations

Station	Parameter	V. observed	L. observed	T. observed	Simulated
Ahar	PGA (cm/s^2)	92	196	267	235
	PGV (cm/s)	4.0	6.9	14.2	13.9
	PGD (cm)	0.9	2.2	1.6	2.1
Varzaghan	PGA (cm/s^2)	211	441	348	369
	PGV (cm/s)	12.6	49.1	26.2	44.5
	PGD (cm)	4.3	11.0	11.1	11.5
Khajeh	PGA (cm/s^2)	96	202	284	210
	PGV (cm/s)	9.1	9.9	20.1	16.8
	PGD (cm)	3.1	3.9	4.8	3.1
Meshkin Shahr	PGA (cm/s^2)	30	56	49	55
	PGV (cm/s)	1.2	3.0	2.6	4.1
	PGD (cm)	0.3	1.3	0.7	0.8
Damirchi	PGA (cm/s^2)	39	91	81	91
	PGV (cm/s)	1.0	2.0	2.0	3.4
	PGD (cm)	0.4	0.5	0.5	0.9
Hoorand	PGA (cm/s^2)	41	66	53	52
	PGV (cm/s)	1.5	2.0	1.7	3.2
	PGD (cm)	0.4	0.7	0.5	1.2

9 Conclusions

In the current study, horizontal components of acceleration ground motion are simulated for the August 11, 2012, M_w 6.4 Ahar earthquake based on stochastic finite-fault approach at six stations. Based on the slop of curved amplitude of Fourier amplitude spectra at higher frequencies, k_0 for horizontal and vertical components are calculated equal to 0.02 and 0.05 s, respectively. A significant difference of the k_0 values shows that the near-surface site attenuation for horizontal components is stronger and more significant than that of the vertical components. Furthermore, horizontal to vertical spectra ratio (H/V) of accelerograms is used to estimate the site effects, including amplification coefficients at different frequencies. Since the kappa value has already been included in the H/V ratio spectra, the $\frac{H}{V}$ exp $(-\pi f k v)$ function is applied to estimate site amplification. What is more, the wavelet-based analysis is used to estimate path-dependent Q_s values at six stations which are mainly derived from the vertical components to avoid the site effects. For this purpose, the researcher rewrote the anelastic attenuation form $\exp(-\pi f D/Q\beta)$ of Eq. (4) as $A(t)=A0\exp(-\pi f t/Q)$ for each frequency in time domain. The attenuating rate is calculated for each frequency

separately and is written in general form as $Q = Q_0 f^n$ by using the least-squares fit. The average of Q is considered as $Q=(122\pm38)f^{(1.40\pm0.16)}$ which is similar to the relation of $Q=87e^{1.46}$ that was proposed for north of Iran (Motazedian 2006). Simulation results represent their conformity as well. Other parameters are also considered based on Motazedian (2006) (Table 4).

After estimating the specific regional key parameters, the stochastic approach based on dynamic frequency model is applied to predict the ground motion of the Ahar earthquake. Best results are obtained for stress drop of 70 bars by comparing peak ground motion (PGA, PGV, and PGD). The results are illustrated in Figs. 5 and 6 and summarized in Table 5. The comparison of waveforms between observed and simulated response spectra shows good agreement.

In addition, there is good conformity between Motazedian (2006) specific key parameters with the obtained results. It shows that it is possible to use them in order to simulate ground motion of possible earthquake scenarios in northern Iran. For example, the metropolis of Tehran is known to have high potential for seismic activities due to many active faults in the same area and there are not any significant earthquake records for engineering studies undertaken in Tehran. This study
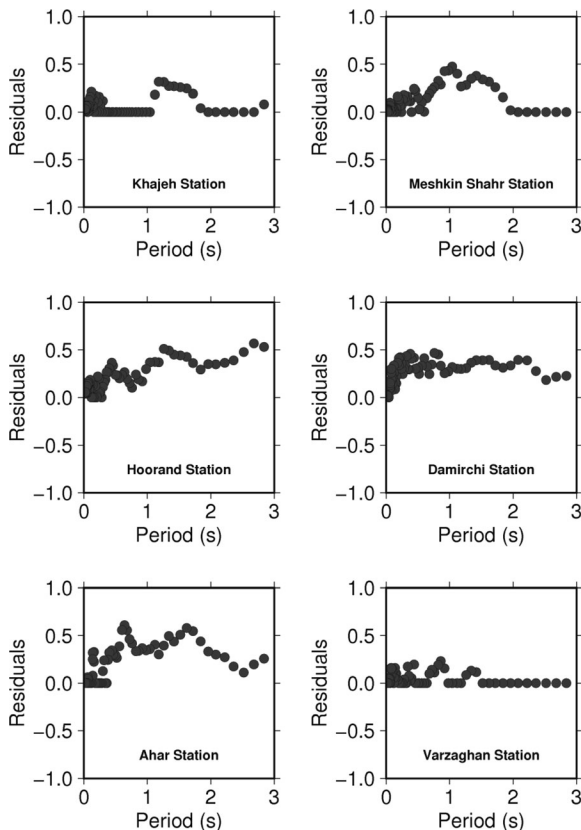
Fig. 6 The distribution of residuals versus frequency contents. Residual is defined as the log of observed response spectra (the geometric mean of the two horizontal components) minus the log of simulated response spectra in six target stations

strongly recommends that key parameters proposed by Motazedian (2006) can be used in order to predict future ground motions in the north of Iran.

10 Data and resources

The strong-motion data used in this project were provided by the National Strong Motion Network of Iran under management of Building and Housing Research Center of the Ministry of Housing and Urban Development of Iran.

The figures were also prepared by using Generic Mapping Tools (Wessel and Smith 1998).

References

Aki K (1967) Scaling law of seismic spectrum. J Geophys Res 72: 1217–1231

Aki K (1980) Attenuation of shear-waves in the lithosphere for frequencies from 0.05 to 25 Hz. Phys Earth Planet Inter 21: 50–60

Ambraseys NN, Melville CP (1982) A history of Persian earthquakes. Cambridge earth science series. Cambridge University Press, London, 212 pp

Anderson JG, Hough SE (1984) A model for the shape of the Fourier amplitude spectrum of acceleration at high frequencies. Bull Seismol Soc Am 74:1969–1993

Atkinson GM (2004) Empirical attenuation of ground-motion spectral amplitudes in southeastern Canada and the northeastern United States. Bull Seismol Soc Am 94:1079–1095

Atkinson GM, Cassidy J (2000) Integrated use of seismograph and strong motion data to determine soil amplification in the Fraser Delta: results from the Duvall and Georgia Strait earthquakes. Bull Seismol Soc Am 90:1028–1040

Berberian M (1976) Contribution to the seismotectonics of Iran (Part II). Geol Surv Iran Report No. 39:516 pp

Berberian M (1994) Natural hazards and the first earthquake catalog of Iran. vol. 1: historical hazards in Iran prior 1900. I.I.E.E.S. report

Berberian M, Yeats RS (1999) Patterns of historical rupture in the Iranian plateau. Bull Seismol Soc Am 89:120–139

Beresnev IA, Atkinson GM (1997) Modeling finite-fault radiation from the omega (super n) spectrum. Bull Seismol Soc Am 87: 67–84

Beresnev I, Atkinson GM (1998) Stochastic finite-fault modeling of ground motions from the 1994 Northridge, California earthquake. I. Validation on rock sites. Bull Seismol Soc Am 88:1392–1401

Bolourchi MJ, Solaymani N, Faridi M, Oveisi B, Ghalamghash J, Sartipi N (2012) Preliminary report of 2012 Aug. 11 Ahar-Varzaghan earthquake, NE Iran. Geological Survey of Iran (GSI), internal report (in Persian), http://www.gsi.ir

Boore DM (1983) Stochastic simulation of high-frequency ground motions based on seismological models of the radiated spectra. Bull Seismol Soc Am 73:1865–1894

Boore DM, Joyner WB (1997) Site amplifications for generic rock sites. Bull Seismol Soc Am 87:327–341

Copley A, Jackson J (2006) Active tectonics of the Turkish-Iranian Plateau. Tectonics 25. doi:10.1029/2005TC001906

Copley A, Faridi M, Ghorashi M, Hollingsworth J, Jackson J, Nazari H, Oveisi B, Talebian M (2013) The 2012 August 11 Ahar earthquakes: consequences for tectonics and earthquake hazard in the Turkish–Iranian Plateau. Geophys J Int. doi:10.1093/gji/ggt379

Daubechies I (1992) Ten lectures on wavelets, the society of industrial and applied mathematics

Hartzell S (1978) Earthquake aftershocks as Green's functions. Geophys Res Lett 5:1–14

Heaton T, Hartzell S (1986) Source characteristics of hypothetical subduction earthquakes in the northwestern United States. Bull Seismol Soc Am 76:675–708

Hessami K, Pantosti D, Tabassi H, Shabanian E, Abbassi MR, Feghhi K, Solaymani S (2003) Paleoearthquakes and slip

rates of the North Tabriz Fault, NWIran: preliminary results. Ann Geophys 46:903–915

Irikura K, Kamae K (1994) Estimaion of strong ground motion in broad-frequency band based on a seismic source scaling model and an empirical Green's function technique. Ann Geophys XXXVII(6):25–47

Jackson J (1992) Partitioning of strike-slip and convergent motion between Eurasia and Arabia in Eastern Turkey and the Caucasus. J Geophys Res 97:471–12479

Joyner WB, Boore DM (1986) On simulating large earthquakes by Green's function addition of smaller earthquakes, in Earthquake source mechanics. American Geophysical Union Geophysical Monograph Washington D.C., 37, 269–274

Lermo J, Chavez-Garcia F (1993) Site effect evaluation using spectral ratios with only one station. Bull Seismol Soc Am 83:1574–1594

Mallat S (1999) A wavelet tour of signal processing. Academic, San Diego

McClusky S, Balassanian S, Barka A, Demir C, Ergintav S, Georgiev I, Gurkan O, Hamburger M, Hurst K, Kahel H, Kastens K, Kekelidze G, King R, Kotzev V, Lenk O, Mahmoud S, Mishin A, Nadariya M, Ouzounit A, Paradissis D, Peter Y, Prilepin M, Reilinger R, Sanli I, Seeger H, Tealeb A, Toksoz MN, Veis V (2000) Global positioning system constraints on plate kinematics and dynamics in the eastern Mediterranean and Caucasus. J Geophys Res 105:5695–5719

Mirzaei N, Gao MT, Chen YT (1999) Delineation of potential seismic sources for seismic zoning of Iran. J Seismol 1:17–30

Motazedian D (2006) Region-specific seismic parameters for earthquakes in northern Iran. Bull Seismol Soc Am 96:1383–1395

Motazedian D, Atkinson GM (2005) Stochastic finite-fault modeling based on a dynamic corner frequency. Bull Seismol Soc Am 95:995–1010

Mousavi M, Zafarani H, Rahpeyma S, Azarbakht A (2014) Test of goodness of the NGA ground-motion equations to predict the strong motions of the 2012 Ahar-Varzaghan dual earthquakes in northwestern Iran. Bull Seismol Soc Am 104. doi:10.1785/0120130302

Nakamura Y (1989) A method for dynamic characteristics estimation of subsurface using microtremor on the ground surface. QR RTRI 30:25–33

Nowroozi AA (1976) Seismotectonic provinces of Iran. Bull Seismol Soc Am 66:1249–1276

Raoof M, Herrmann R, Malagnini L (1999) Attenuation and excitation of three-component ground motion in southern California. Bull Seismol Soc Am 89:888–902

Siddiqqi J, Atkinson GM (2002) Ground motion amplification at rock sites across Canada, as determined from the horizontal-to-vertical component ratio. Bull Seismol Soc Am 92:877–884

Sokolov VY, Loh CH, Wen KL (2002) Comparison of the Taiwan Chi-Chi earthquake strong-motion data and ground-motion assessment based on spectral model form smaller earthquakes in Taiwan. Bull Seismol Soc Am 92:1855–1877

Solaymani Azad S, Dominguez PH, Hessami S, Shahpasandzadeh K, Forutan Tabassi MR, Lamothe M (2010) Paleoseismological andmorphological evidences of slip ariations along the North Tabriz Fault (NWIran), preprint

Vernant P, Nilforoushan F, Hatzfeld D, Abassi MR, Vigny C, Masson F, Nankali H, Martinod J, Ashtiani M, Bayer R, Tavakoli F, Chéry J (2004) Present-day crustal deformation and plate kinematics in the Middle East constrained by GPS measurements in Iran and northern Oman. Geophys J Int 157:381–398

Wells D, Coppersmith K (1994) New empirical relationships among magnitude, rupture length, rupture width, ripture area and surface displacement. Bull Seismol Soc Am 84:974–1002

Wessel P, Smith WHF (1998) New, improved version of Generic Mapping Tools released. EOS Trans AGU 79:579

Zare M, Bard PY, Ghafory-Ashtiany M (1999) Site characterizations for the Iranian strong motion network. Soil Dyn Earthq Eng 18:101–123